DOI: 10.15669/pnst.7.117

Progress in Nuclear Science and Technology
Volume 7 (2025) pp. 117-121

ARTICLE

Stroboscopic X-ray imaging technique with optically chasing accelerator operation for mechanically driven sample

Tatsunori Shibuya [a, b, *], Yuya Koshiba [c, d], Yuichi Tadenuma [c], Sena Maru [b, c], Masakazu Washio [c], Takeshi Fujiwara [a], Ryunosuke Kuroda [a, b] and Nagayasu Oshima [a]

[a] *Research Institute for Measurement and Analytical Instrumentation, National Metrology Institute of Japan, National Institute of Advanced Industrial Science and Technology, 1-1-1 Umezono, Tsukuba 305-8568, Japan;* [b] *AIST-UTokyo Advanced Operando-Measurement Technology Open Innovation Laboratory, National Institute of Advanced Industrial Science and Technology, 5-1-5 Kashiwanoha, Kashiwa, Chiba 277-8561, Japan;* [c] *Waseda Research Institute for Science and Engineering (WISE), Waseda University, 3-4-1 Okubo, Shinjuku, Tokyo 169-8555, Japan;* [d] *HiLASE Centre, Institute ofPhysics CAS, Za Radnicí 828, 252 41 Dolní Břežany, Czech Republic*

Optimizing the design of mechanically driven samples is a crucial for carbon dioxide emission reduction. These instruments are generally made of optically invisible materials, such as a structural body of iron or aluminum, neodymium or ferrite as a magnetic material, coil of copper, and some oil types. In addition, the clocking accuracy of these instruments has a timing jitter up to 10 % during operation. That is, the imaging technique for this instrument requires high transmissibility and dynamic operation with chasing sample clocking. In this study, we developed a triggering method based on an optical system for RF-type accelerator operation and applied it to stroboscopic high-energy X-ray imaging. We report stroboscopic X-ray imaging with a clear rotational motion of the motor instrument sample up to a rotational speed of 4200 rpm and an analysis method that takes advantage of its rotational phase in one cycle. These procedures can potentially be applied for lifetime measurements and defect inspection of mechanically driven samples.

Keywords: X-ray imaging; stroboscopic imaging; accelerator

1. Introduction

Stroboscopic X-ray imaging is emerging as an essential measurement technique for evaluating motors or engines for carbon dioxide emission reduction [1-3]. This is because in situ [4,5] or operando [6,7] X-ray measurements ultimately determine the optimality of a unique assembly equipment composed of opaque composites, such as iron and aluminum structures, neodymium or ferrite magnets, copper coils, and lubricating oils. However, the cyclic motion of these instruments has a timing jitter up to 10 %; therefore, a triggering method is required for precise measurements. Currently, triggering methods are based on an acoustic, electric, magnetic, and optical system [8-10], which has a typical rise time of several nanoseconds. These techniques have been used in high-energy X-ray tubes [8] and synchrotron radiation facilities [11]. Very recently, X-ray techniques are required with a temporal resolution of sub-microseconds, in which measurement objects have high-speed rotational motion with speeds up to 50,000 rpm [12,13]. The radiofrequency (RF) gun with MHz femtosecond laser-based operation [14] guarantees this temporal quality, making it an attractive combination for this triggering method for use in high-speed object measurements.

Particle accelerators are typically controlled by RF systems; signal-based RF systems consist of an RF reference signal, low-level RF (LLRF), pre-amplifier, and klystron. The output power is milliwatt at LLRF, watt-level at pre-amplifier, and over 100 kW at klystron, which finally leads to an accelerating cavity. Of these, signal synchronization is distributed from the master oscillator installed in the LLRF part to the pulse modulator, timing modulator, local oscillator, etc., and synchronization for control of the entire system is performed at the point of the master oscillator within the LLRF. Specifically, by feeding the reference signal from the outside to the master oscillator, it is possible to eliminate effects other than the timing jitter inside the accelerator.

Our system optically detects the measuring target, which is usually an independent system that can be accessed from the external side. The advantage of the optical method is that the recent development of laser diodes has made it possible to realize compact systems. In addition, the rotational driving part is exposed to the outside, making it possible to use the original design such as an optical chopper or slit. The optical method, which transmits to the beam diameter at the spatial light focus,

*Corresponding author. E-mail: t-shibuya@aist.go.jp

has a lower timing jitter at the trigger point because of the high spatial coherence of the single-mode fiber-coupled laser diode. Therefore, the adoption of tabletop X-ray imaging from a photocathode RF-gun is a reasonable choice with regard to material transparency, temporal resolution, and accessibility of X-ray generation. In this study, we report that an RF accelerator with optical triggering is operated to synchronize X-ray generation for stroboscopically imaging the motor sample under operation and the analysis for utilizing its triggering characteristics.

2. Instrument performance

A concrete example is as follows: Assuming the measurement of an object rotating at a maximum of tens of thousands of rpm (several milliseconds per cycle) with an accuracy of ±0.1°, an electron pulse width of sub-microsecond, that is, 100 to 1000 electronic pulse trains, is required. Furthermore, the X-ray energy should be in the range of 100 keV to 1 MeV for sufficient penetration power. Our X-ray generator is mainly composed of an RF gun with an S-band system (2856 MHz), a synchronized fiber laser, an optically chasing system, and an unsynchronized X-ray flat panel detector; the RF gun provides an energy of 5 MeV, bunch charge of 150 pC, repetition rate of 5 Hz, and pulse duration of 2.5 ps (FWHM), and the number of bunches are 100. The accelerator system and the fiber laser system were synchronized at 119 MHz, the laser pulse was converted to fourth harmonics through two nonlinear crystals, and the harmonics led to the cathode surface for photoemission [15,16].

The generated electron beam was accelerated and focused on a tantalum target with a thickness of 0.5 mm using doublet quadrupole magnet. According to Ref. [17], the conversion rate from electrons to bremsstrahlung is approximately assumed to be 15%. Then, the bremsstrahlung pulse was filtered using a carbon block of 50 mm thickness for removing the low-energy radiation, so the peak energy of the filtered pulse was assumed to be 1 MeV. To confirm that the generated X-rays contained high-energy components, we conducted a transmission test of X-rays through a steel plate (ss400) with a thickness of 45 mm. Note that no steel plate was set in the practical imaging experiment. Finally, the emitted X-rays were detected behind a brushed DC motor, which is a typical electrically driven motor with 3-phase and 2-pole. The motor had a diameter of 35.6 mm. For phase detection, a ring marker made of SUS304 weighing 1.7 g was held on a slit plate made of aluminum, which has the plate thickness of 1 mm and the slit of 5 mm, at a point 29.3 mm from the center of the motor, as shown in **Figure 1**. The motor was operated at approximately 70 Hz (equivalent to 4200 rpm) and its rotational frequency was measured using a frequency counter (HEWLETT PACKARD: 5350B Microwave Frequency Counter). The X-ray detector had a pixel size of 200 μm and a detector size of 310 mm × 256 mm in the 16-bit mode [18,19]. The magnification calculated from the motor diameter was 2.0, and the spatial resolution obtained from the image edge blur was 0.3 mm. The resolution was mainly determined by the electron beam size on the target.

The optical triggering system comprises a laser diode (LD), slit plate, and photodiode (PD). The LD and driver were prepared using Thorlabs LP780-SAD15 and Thorlabs CLD1011LP, respectively. The PD used was Koheron: PD200T with TTL analog signal, which was input directly to the signal generator (SG). Subsequently, the SG was output as an RF reference signal of 5 Hz for accelerator operation. Eventually, a conceptual diagram of the experimental system was constructed, as shown in Figure 1.

3. Validation experiment and discussion

As a validation experiment, images obtained using the proposed method, as shown in Figure 1, and a conventional accelerator operation method were compared. More

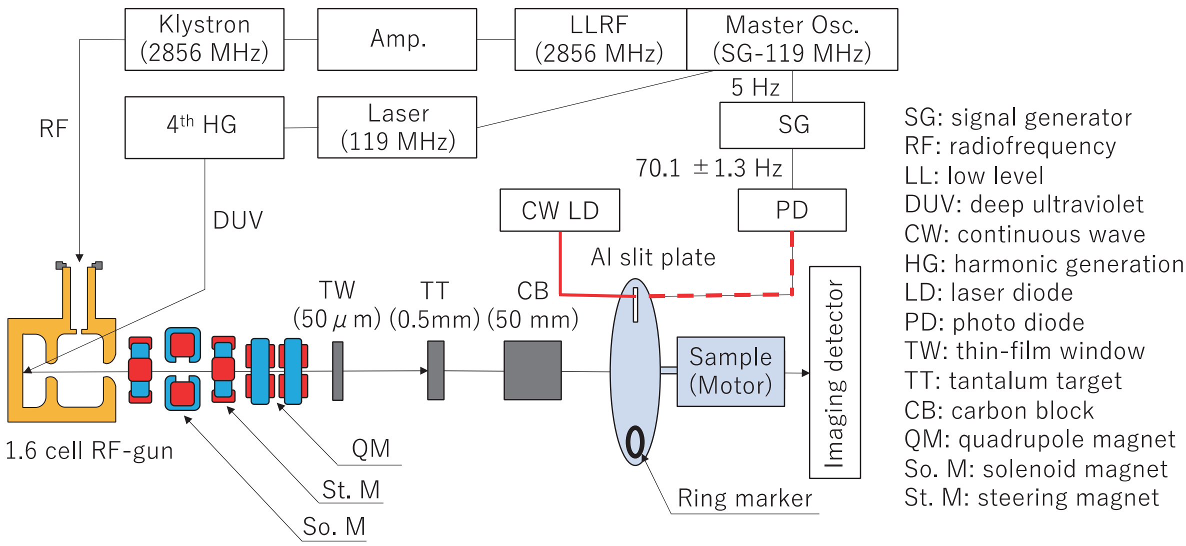

Figure 1. Schematic of the experimental setup to image the rotating sample.

specifically, in the conventional accelerator system, the LD, PD, and SG parts were not installed, as shown in Figure 1; instead, the power source based on the wall plug was installed in the SG part. In the compared threshold images shown in **Figure 2**, the motor shape near the center of (a) can be clearly visualized, while that of (b) is smeared. In Figure 2, these obtained original images were treated a threshold with 34% of the maximum value and 18% of the minimum value. The number of accelerations and decelerations within one rotation depends on the motor structures with multipolar magnets, and the amplitude of fluctuation is affected by the structural symmetry, that is, the misalignment of motor details, such as the commutator, rotor coils, stator magnets, and winding stator. Because there is a causal relationship between the structural properties and a period jitter, it is natural that these accelerations/decelerations cause variability factors in brushless motors or other magnetic motors. In addition, an electrical driver circuit is also important, and there is a possibility that the rotation speed will fluctuate due to fluctuations in the drive current, owing to the power generation effect peculiar to the motor. Our proposal is based on the sample-triggering method and motion phase analysis, in which the phase ϕ is defined as follows:

$$\phi = \omega\tau + \theta. \qquad (1)$$

Where θ corresponds to the initial phase at $\omega\tau = 0$ and $\theta = 0$ in this paper, and ω is angular frequency and $\omega\tau$ represents the phase fluctuation as delay time τ. Strictly, measurements at phase "zero" are subject to electrical and optical delays, but the initial delay of an electrical signal is much faster than the mechanical rotational motion speed. Therefore, even if we compare each image at $\omega\tau = 0$, we cannot confirm the differences in the images. However, if the phase is changed by manipulating the delay time, there is a phase fluctuation due to rotational motion, and the integral image fluctuates.

Representative X-ray images obtained at two different delay times based on the optically chasing sample-triggering method are shown in **Figures 3(a)** and **(b)**. The

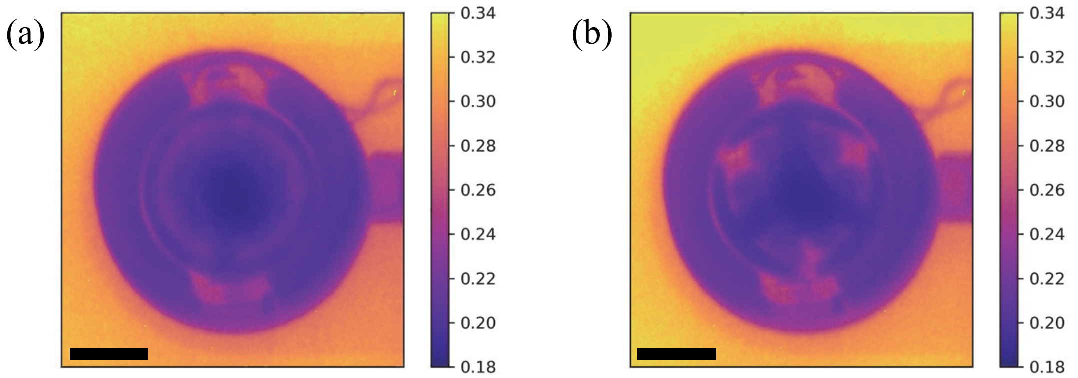

Figure 2. Comparison of X-ray radiography threshold images at $\omega\tau = 0$ for the motor instrument sample under operation with a master oscillator setting of (a) optically chasing sample triggering method and (b) conventional accelerator triggering method. These images include with all background noises. The scale bar corresponds to 10 mm.

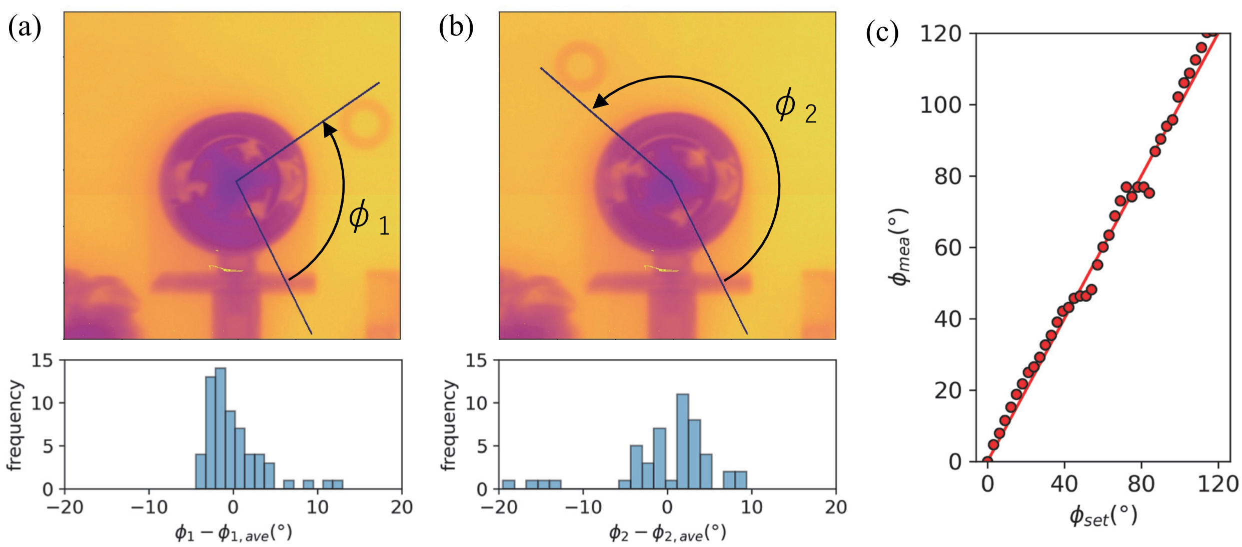

Figure 3. Comparison of X-ray images for $\phi = \phi_1$ (a) and $\phi = \phi_2$ (b). (c) Correlation of set phase ϕ_{set} and the measured phase ϕ_{mea}. The set phase is calculated by setting the delay time in SG.

measurements in Figures 3(a) and (b) were obtained with 50 and 58 times every 10-s exposure, respectively. Since the double-ring structure smeared by large phase fluctuations were not able to be counted, the 48 times of ϕ_1 and 57 times of ϕ_2 are judged to be appropriate of analysis as shown in Figures 3(a) and (b)'s histogram. Additionally, to improve the visualization of the image, the upper limit of the maximum value was set to the original maximum value of 91 % in Figure 3(a) and 76% in Figure 3(b) by adjusting the dynamic range. These phases were obtained by finding the tangent of the ring marker to the center of motor. From these measurements, the average phases of Figures 3(a) and 3(b) were obtained as $\phi_1 = 97.0°$ and $\phi_2 = 203.8°$, respectively. Essentially, the only known value is the delay time set in the SG, and the set phase ϕ_{set} and measured phase ϕ_{mea} can be compared, as shown in Figure 3(c). The exposure time was 10 s, and the phase was stepped and measured every 3°. A phase shift of deceleration was observed near $54°$ and $84°$, which caused from fluctuating currents of imperfect feedback circuit between motor head and drive circuit, even though no periodic regularity was found.

The phase fluctuations shown in Figures 3 are potentially useful for quality assurance and aging-derived life measurements. In other words, by time-monitoring the difference between the set phase and the measured phase, failure or life can be identified if the fluctuation range of the difference is larger than the normal fluctuation range. In this experiment, the number of measurements of the phase was 50 to 60, but it was necessary to improve the accuracy of determining the average phase, that is, the accuracy of $\omega\tau$ obtained from the measurement.

Our experimental technique was applied to targets with rotational speeds of up to 4200 rpm, but there are no technical hurdles to its application to a bearing system with tens of thousands of rpm. In short, these techniques enable the dynamic measurements of advanced assembly equipment. Additionally, by applying Fourier analysis to such phase detection, it may be possible to search for factors that contribute to abnormal operation and equipment life owing to a specific frequency that deviates from the reference frequency determined by the rotation speed. In particular, the proposed technique is highly compatible with stroboscopic methods with an extremely low timing jitter, suggesting the possibility of leading to important analyses. This scope of application exists not only in motors but also in bearings and engine structures, which potentially exist in various measurement objects with asymmetric structures and heat source effects. Our proposed method and system can be extended to high-speed imaging [5] next step.

4. Conclusion

We demonstrated the stroboscopic X-ray imaging with optically chasing operation for a mechanically driven sample. This technique allows the visualization of phase slipping at acceleration and deceleration in each rotational motion. This result shows to apply to industrial assembly for advanced imprecision and lifetime measurement.

Acknowledgements

This work was supported in part by JSPS KAKENHI (Grant Numbers JP21K20361 and JP22K18133) and in part by JST (ACT-X Grant Number JPMJAX22K7, Japan).

References

[1] J. Ren, R. Ren, M. Green and X. Huang, Defect Detection from X-Ray Images Using A Three-Stage Deep Learning Algorithm, *IEEE Canadian Conference of Electrical and Computer Engineering (CCECE)* (2019), pp. 1-4.

[2] J.D. Rogers, Measurement of dimensional changes and movements in engineering components using x-ray radiographic imaging, *Meas. Sci. Technol.* 11 (2000), pp. 857-864.

[3] B. Schillinger, J. Brunner and E. Calzada, A study of oil lubrication in a rotating engine using stroboscopic neutron imaging, *Physica B Condens. Matter* 385-386 (2006), pp. 921-923.

[4] B. Bazin, M.T. Bieber, C. Roque and M. Bouteca, Improvement in the Characterization of the Acid Wormholing by "In Situ" X-Ray CT Visualizations (SPE, 1996), p. SPE–31073–MS.

[5] C.L.A. Leung, S. Marussi, R.C. Atwood, M. Towrie, P.J. Withers and P.D. Lee, In situ X-ray imaging of defect and molten pool dynamics in laser additive manufacturing, *Nat. Commun.* 9 (2018), p. 1355.

[6] A. Johannes, D. Salomon, G. Martinez-Criado, M. Glaser, A. Lugstein and C. Ronning, In operando x-ray imaging of nanoscale devices: Composition, valence, and internal electrical fields, *Sci. Adv.* 3 (2017), eaao4044.

[7] L. Wang, J. Wang and P. Zuo, Probing Battery Electrochemistry with In Operando Synchrotron X-Ray Imaging Techniques, *Small Methods* 2 (2018), 1700293.

[8] B.J. Vincent, Stroboscopic radiography with a linear accelerator, *Br. J. Appl. Phys.* 11 (1960), pp. 132-135.

[9] T. Kanaji, K. Yasuda, S. Ikuta and M. Takeda, Pulsed X-Ray Radiography with Electron Linear Accelerator (I) Precise Control of Electron Linear Accelerator, *Jpn. J. Appl. Phys.* 7 (1968), pp. 102-111.

[10] Y. Cheng, J. Zhang, Y.Z. Lee, B. Gao, S. Dike, W. Lin, J.P. Lu and O. Zhou, Dynamic radiography using a carbon-nanotube-based field-emission x-ray source, *Rev. Sci. Instrum.* 75 (2004), pp. 3264-3267.

[11] N. Baimpas, M. Drakopoulos, T. Connolley, X. Song, C. Pandazaras and A.M. Korsunsky, A feasibility study of dynamic stress analysis inside a running internal combustion engine using synchrotron X-ray beams, *J. Synchrotron Radiat.* 20 (2013), pp. 316-323.

[12] J. Tribol., Analysis of an Aerodynamic Compliant Foil Thrust Bearing: Method for a Rapid Design, 121 (1999), pp. 816-822.

[13] S. Kulkarni, S.D. Naik, K.S. Kumar, M. Radhakrishna and S. Jana, Development of Foil Bearings for Small Rotors, in *Gas Turbine India Conference* (American Society of Mechanical Engineers, 2013), p. V001T05A010.

[14] K. Sakaue, H. Hayano, S. Kashiwagi, R. Kuroda, A. Masuda, T. Suzuki, T. Takatomi, N. Terunuma, J. Urakawa and M. Washio, Cs-Te photocathode RF electron gun for applied research at the Waseda University, *Nucl. Instrum. Methods Phys. Res. B*, 24 (2011), pp. 2928-2931.
[15] K. Sakaue, Y. Nishimura, M. Nishiyama, T. Takahashi, M. Washio, T. Takatomi and J. Urakawa, Temporal profile measurement of an electron bunch with the two-cell rf deflecting cavity at Waseda University, *Jap. J. Appl. Phys.* 54 (2015), 026301-1-6.
[16] Y. Koshiba, Y. Tadenuma, S. Otsuka, M. Washio, T. Takatomi, J. Urakawa and K. Sakaue, High-charge ultrashort electron bunch generation by an energy chirping cell-attached rf electron gun and its measurement using a transverse deflecting cavity, *Phys. Rev. AB*. 24 (2021), 083401.
[17] W. Chien-Shiung, The Continuous X-Rays Excited by the Beta-Particles of ${}_{15}P^{32}$, *Phys. Rev.* 59 (1941), pp. 481-488.
[18] T. Fujiwara, H. Miyoshi, Y. Mitsuya, N.L. Yamada, Y. Wakabayashi, Y. Otake, M. Hino, K. Kino, M. Tanaka, N. Oshima and H. Takahashi, Neutron flat-panel detector using In–Ga–Zn–O thin-film transistor, *Rev. Sci. Instrum.* 93 (2022), 013304.
[19] T. Fujiwara, M. Tanaka and R. Kuroda, Review of the Development of Medical Radiation Imaging Detectors at AIST, *NIHON GAZO GAKKAISHI* 61 (2022), pp. 636-642.